

Data Repository Item

Detailed Model Description

We configured GENIE-1 to address questions of end-Permian euxinia as follows. Biological new production is determined based on phosphate restoring in the surface ocean, with nutrients restored towards zero with a six-year time constant after Cameron et al. (2005). Phosphate, dissolved inorganic carbon (DIC), and alkalinity are consumed in the surface ocean and liberated in the ocean interior with an e-folding depth of remineralization calibrated against the modern vertical PO_4^{3-} distribution (Ridgwell et al., 2007). Where oxygen has been depleted by aerobic respiration, anaerobic remineralization proceeds via sulfate reduction. Sulfide is abiotically oxidized through reaction with oxygen according to the kinetic expression of Zhang and Millero (1993).

We added sulfur phototrophy to the BIOGEM module described in Ridgwell et al. (2007). Green and purple anoxygenic phototrophs oxidize sulfide in the absence of oxygen and presence of light. If areas of the photic surface ocean become sulfidic, sulfur phototrophs thrive, as observed in modern chemically stratified environments such as the Black Sea. Similarly, in the model surface ocean sulfur phototrophy becomes the pathway of primary production in sulfidic grid cells, although the magnitude of new production remains controlled by phosphate supply. This productivity also results in biological oxidation of sulfide to sulfate; although elemental S is the more common metabolic end product, oxidation by O_2 follows, yielding the overall reaction we model:



Figure DR1. Map of sea surface temperatures for the model equilibrated with 12x PAL $p\text{CO}_2$.

Figure DR2. Map of sea surface salinity for the model equilibrated with 12x PAL $p\text{CO}_2$.

Figure DR3. Meridional overturning circulation in Sverdrups (Sv) for the model equilibrated with 12x PAL $p\text{CO}_2$.

Figure DR4. Equilibrium surface-water phosphate distribution for simulation with modern phosphate concentrations.

Figure DR5. Export production (particulate organic matter flux in $\text{mol C m}^{-2} \text{yr}^{-1}$) for the modern phosphate simulation equilibrated with 12x PAL $p\text{CO}_2$.

Figure DR6. Export production (particulate organic matter flux in $\text{mol C m}^{-2} \text{yr}^{-1}$) for the 10x modern phosphate simulation equilibrated with 12x PAL $p\text{CO}_2$.

Figure DR7. $[\text{H}_2\text{S}]$ distribution in a cross section through the Panthalassic Ocean for the 10x modern phosphate simulation equilibrated with 12x PAL $p\text{CO}_2$.

Figure DR8. $[\text{O}_2]$ distribution in a cross section through the Panthalassic Ocean for the 10x modern phosphate simulation equilibrated with 12x PAL $p\text{CO}_2$.

Figure DR9. $[\text{PO}_4^{3-}]$ distribution in a cross section through the Panthalassic Ocean for the 10x modern phosphate simulation equilibrated with 12x PAL $p\text{CO}_2$.

Figure DR10. Cross section of ocean temperature through the Panthalassic Ocean for the model equilibrated with 12x PAL $p\text{CO}_2$.

Figure DR11. Cross section of ocean salinity through the Panthalassic Ocean for the model equilibrated with 12x PAL $p\text{CO}_2$.

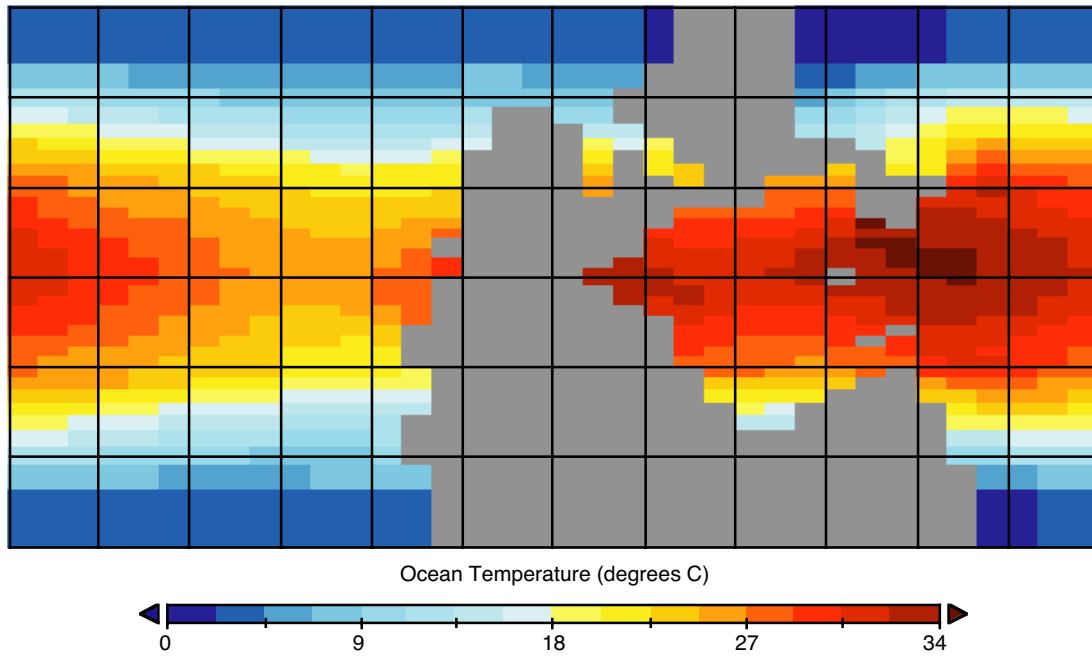
Figure DR1.

Figure DR2.

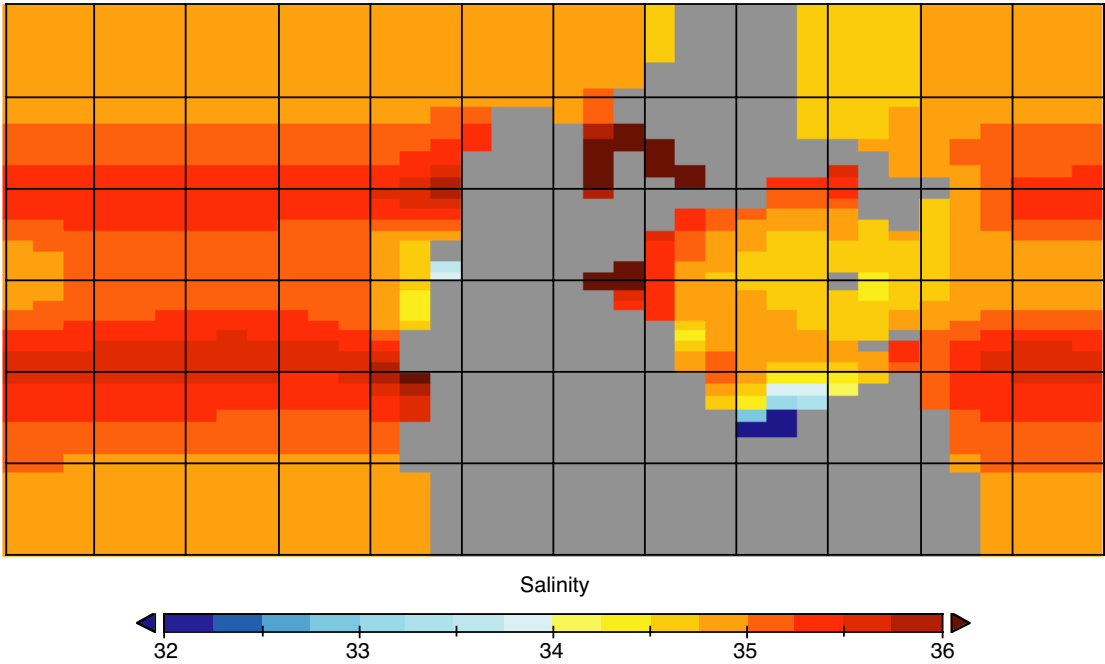


Figure DR3.

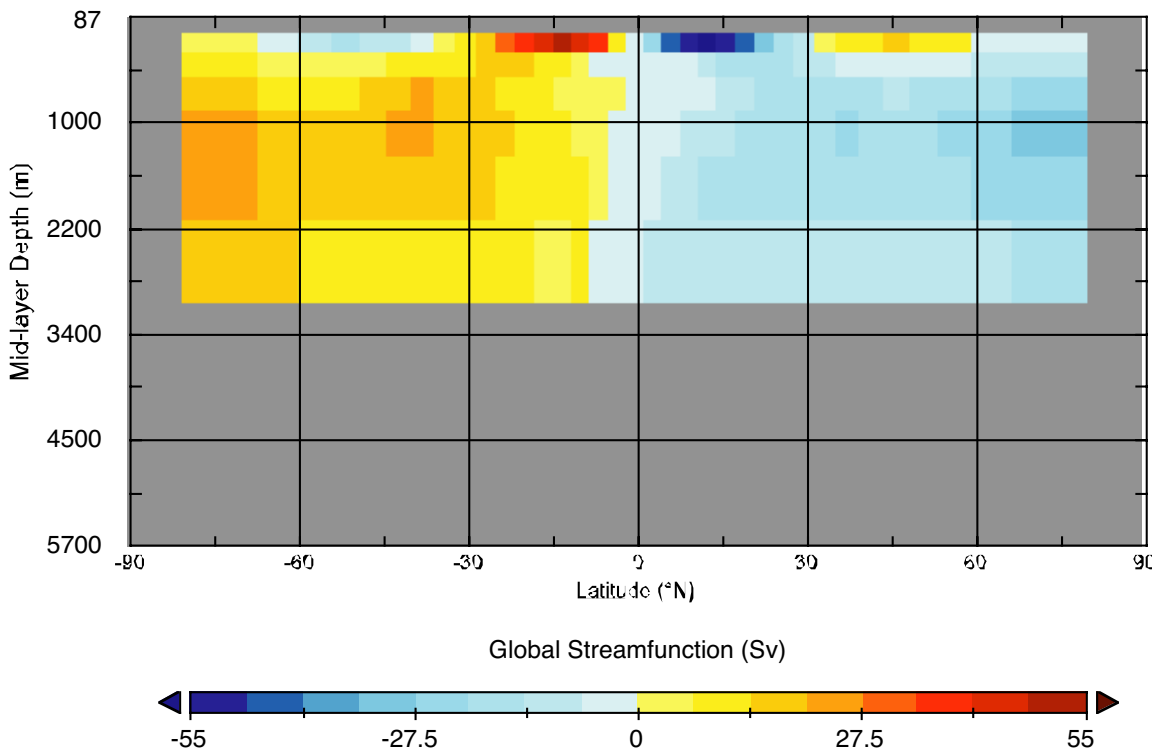


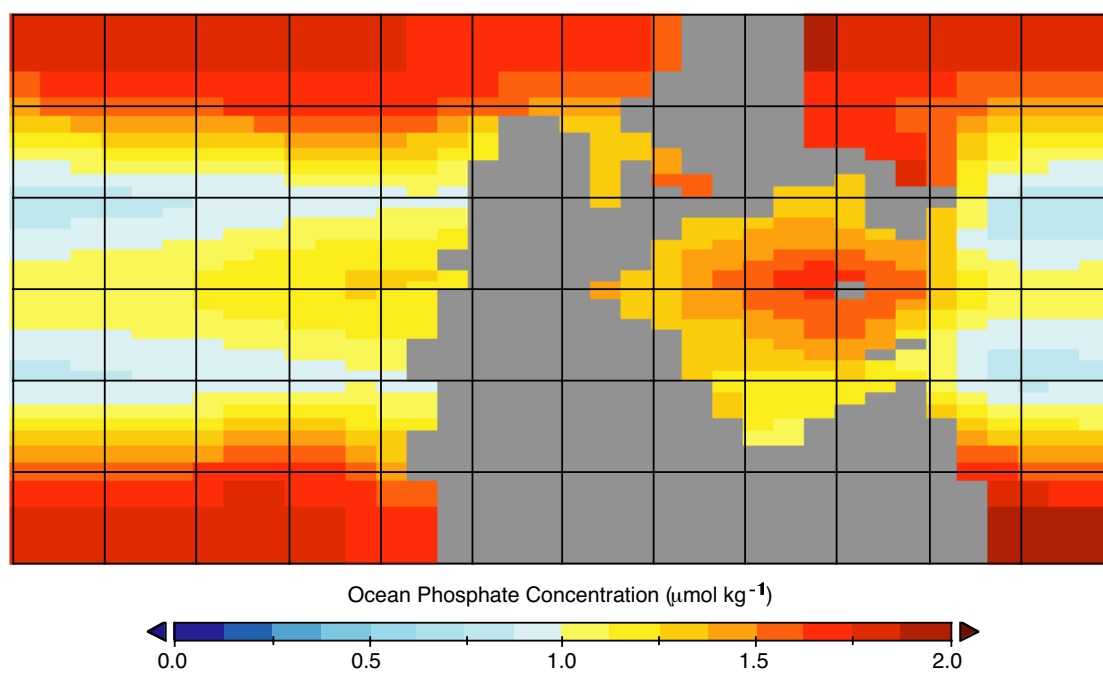
Figure DR4.

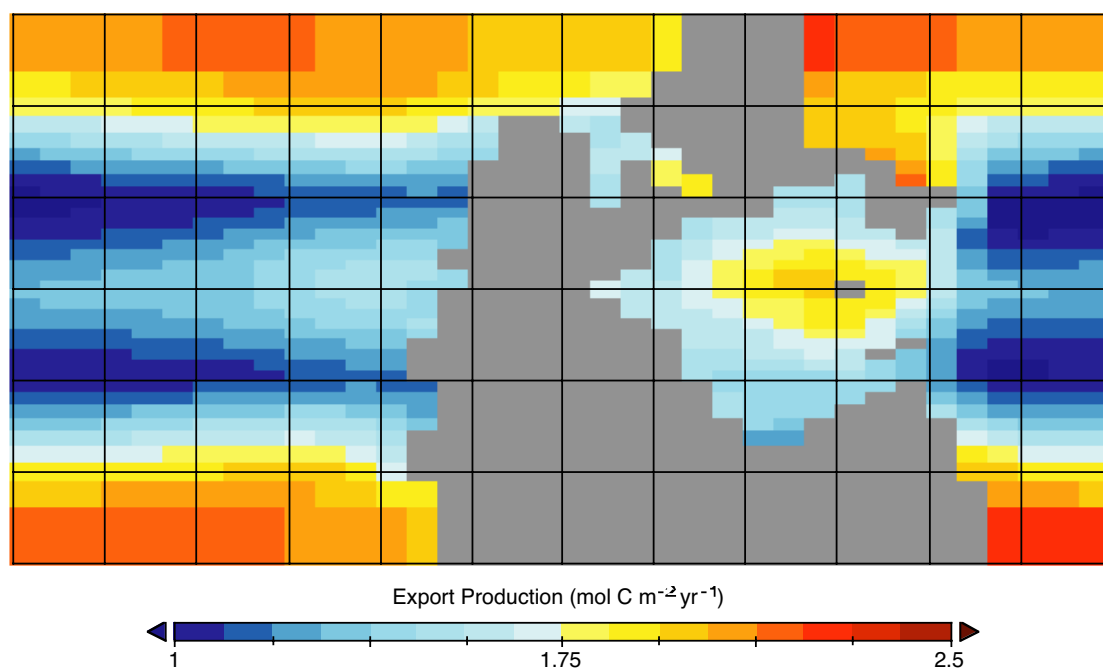
Figure DR5.

Figure DR6.

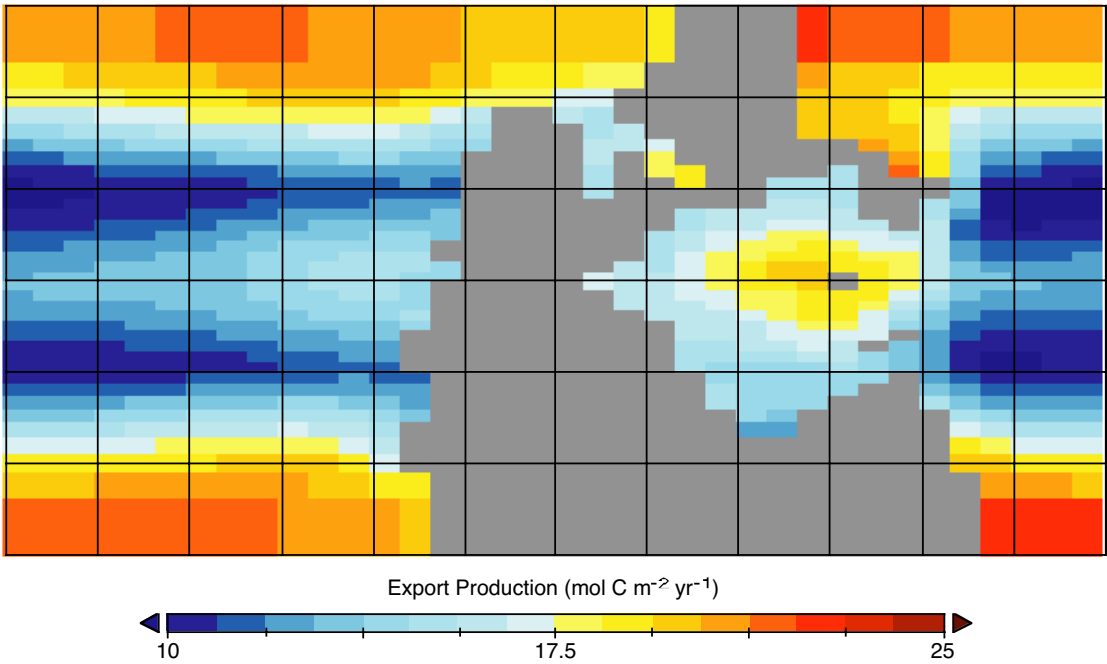


Figure DR7.

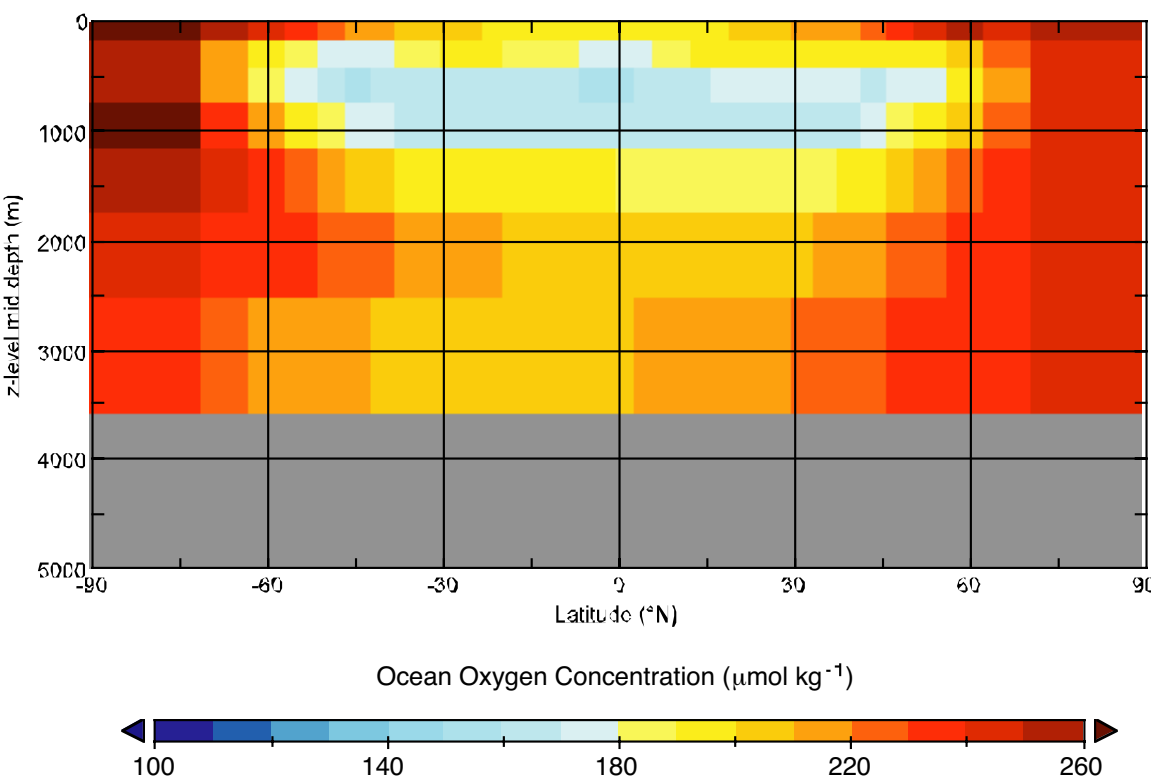


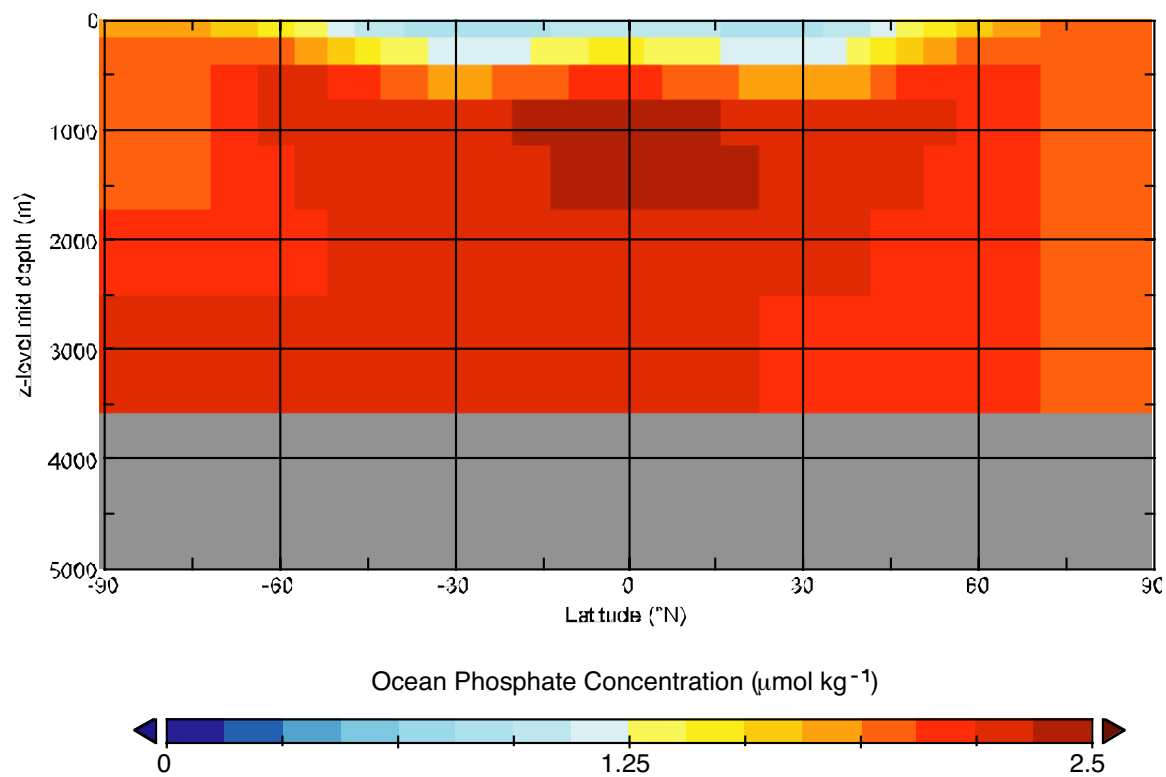
Figure DR8.

Figure DR9.

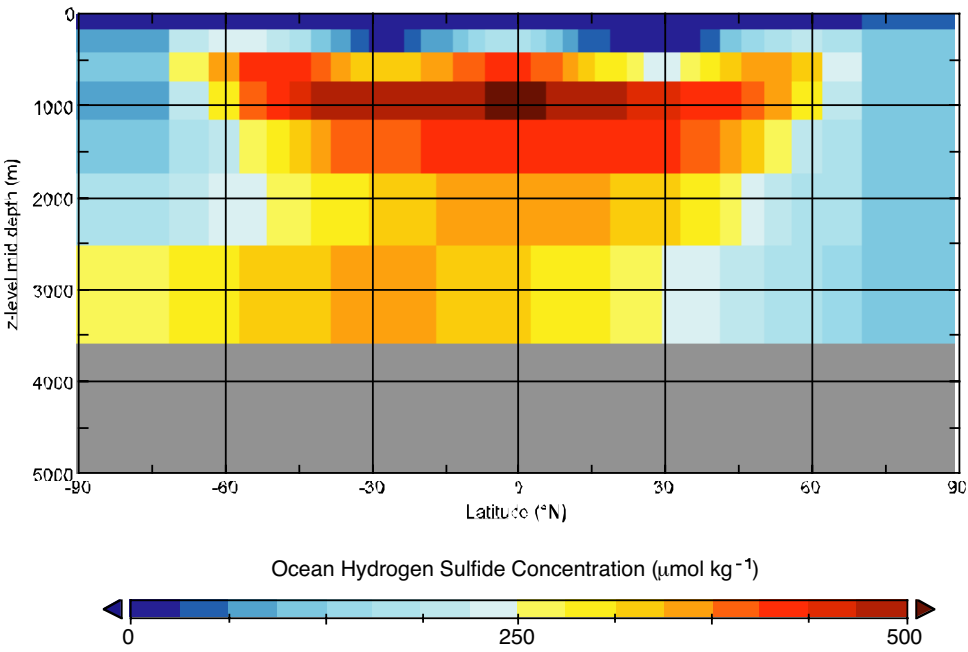


Figure DR10.

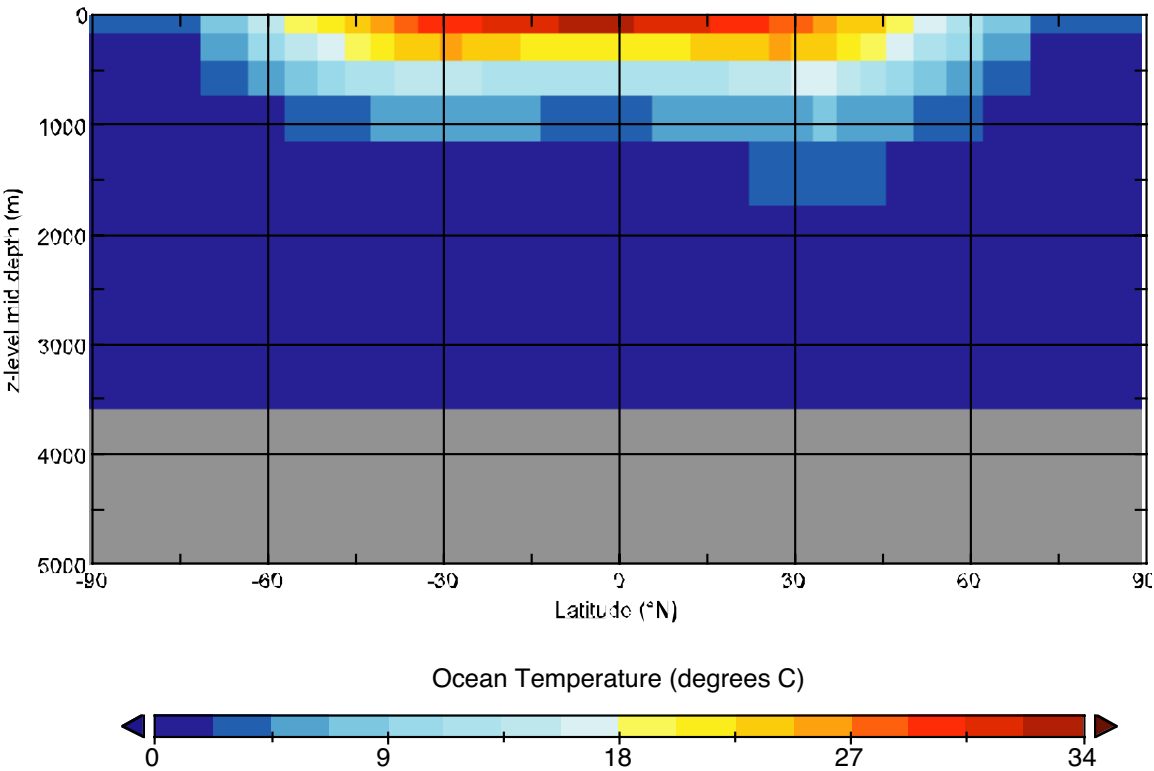


Figure DR11.

